Biosensors and Bioelectronics 123 (2019) 269–277

Contents lists available at ScienceDirect

Biosensors and Bioelectronics

journal homepage: www.elsevier.com/locate/bios

Smartphone-based multicolor bioluminescent 3D spheroid biosensors for monitoring inflammatory activity

Elisa Michelini[a,b,*], Maria Maddalena Calabretta[a], Luca Cevenini[a], Antonia Lopreside[a], Tara Southworth[c], Danielle M. Fontaine[c], Patrizia Simoni[d], Bruce R. Branchini[c], Aldo Roda[a,b,*]

[a] Department of Chemistry "G. Ciamician", University of Bologna, 40126 Bologna, Italy
[b] INBB, Istituto Nazionale di Biostrutture e Biosistemi, 00136 Rome, Italy
[c] Department of Chemistry, Connecticut College, New London, CT 06320, USA
[d] Department of Medical and Surgical Sciences (DIMEC), University of Bologna, Sant'Orsola Malpighi Hospital, Via Massarenti, 9, 40138 Bologna, Italy

ARTICLE INFO

Keywords:
Bioluminescence
Whole-cell biosensor
Luciferase
Smartphone
3D cell model

ABSTRACT

Whole-cell biosensors present many advantages, including being able to monitor the toxicity and bioavailability of chemicals; cells grown in traditional 2D cultures, however, do not reproduce the complexity of in vivo physiology. In the last years, 3D cell-culture models have garnered great attention due to their capability to better mimic in vivo cellular responses to external stimuli, providing excellent model living organisms. In order to obtain a predictive, sensitive, and robust yet low-cost 3D cell biosensor, we developed a smartphone-based bioluminescent 3D cell biosensor platform for effect-based analysis. We exploited the Nuclear Factor-kappa B (NF-kB) signal transduction pathway, which is induced by several types of stressors and is involved in the regulation of cell-cycle/growth, inflammation, apoptosis, and immunity. The smartphone-based biosensor relies on immobilized HEK293 spheroids genetically engineered with powerful red- and green-emitting luciferases utilized as inflammation and viability reporters. It provides a limit of detection for Tumor Necrosis Factor (TNFα) of 0.15 ± 0.05 ng/mL and could be a useful tool to initially screen environmental samples or other compounds on-site, especially for additional more accurate chemical analyses.

1. Introduction

The key idea in turning cells into biosensing systems is to convert molecular recognition events occurring at the cellular and molecular levels into measurable analytical signals (He et al., 2016; Thouand, 2018). In luminescent whole-cell biosensors, this is generally achieved by genetically engineering cells with reporter proteins whose expression is regulated by activation of specific molecular pathways. The expression of reporter proteins can be easily and quantitatively assessed by optical reading, e.g. fluorescence or bioluminescence (BL) (Raut et al., 2012; Roda et al., 2016a; Cevenini et al., 2014).

Thanks to their unusually high detectability, bioluminescent whole-cell biosensors have been used for on-site analysis by integrating cells into portable analytical devices (Michelini and Roda, 2012) exploiting portable light detectors such as charge-coupled devices (CCDs), video cameras, or complementary metal oxide semiconductors (CMOSs). These devices can be classified as true biosensors, since they incorporate entrapped cells as biological recognition elements integrated (or in intimate contact) with a transducer device (Turner, 2013). In the past years whole-cell biosensors, especially those based on robust microbial cells, were successfully applied in diverse fields, ranging from environmental monitoring to food quality assessment and safety analysis (Kim et al., 2018; Bazin et al., 2017; Cevenini et al., 2018; Kabessa et al., 2016; Roggo and van der Meer, 2017; Elad et al., 2010). Nevertheless, problems related to variability in cell growth and metabolism due to uncontrolled factors (e.g., matrix effects, temperature, pH variations) are still unsolved issues that hampered a widespread commercial diffusion of such biosensors.

More recently, portable light detectors have been replaced by smartphone-integrated CMOSs to obtain "instrument-free" detection. Smartphones offer several features that can be exploited for biosensor development, including high computational capability, powerful cameras, high coverage, and data-transmission speed (Zhang and Liu, 2016). Recently, optical microscopes, photometers, and other miniaturizable instrumentation were integrated in smartphones, exploiting 3D printing technology, to obtain reusable or disposable devices providing low-cost alternatives to conventional point-of-need and point-of-care solutions (Comina et al., 2016; Preechaburana et al., 2014; Sicard

* Corresponding authors at: Department of Chemistry "G. Ciamician", University of Bologna, 40126 Bologna, Italy.
E-mail addresses: elisa.michelini8@unibo.it (E. Michelini), aldo.roda@unibo.it (A. Roda).

https://doi.org/10.1016/j.bios.2018.09.012
Received 22 June 2018; Received in revised form 14 August 2018; Accepted 1 September 2018
Available online 04 September 2018
0956-5663/

et al., 2015). Despite its huge potential, the implementation of BL in smartphone-based platforms has been seldom explored (Arts et al., 2016; Cevenini et al., 2016a, 2016b; Ding et al., 2018; Kim et al., 2017; Roda et al., 2014a). It is well known that several advantages of BL are valuable for its implementation as a detection technique into compact portable devices, since no external light source and no geometry requirements for light detection are required (Roda et al., 2016b, 2013). However, it must be pointed out that, despite the excellent signal to noise ratio due to low background and high quantum yield of BL reactions catalyzed by luciferases (e.g., 0.4 for *P. pyralis* luciferase, Niwa et al., 2010), BL signals are generally very weak, challenging the detectors' sensitivity. For this reason, different strategies were undertaken, such as the selection of very bright luciferases (Arts et al., 2016; Ding et al., 2018), and the implementation of custom algorithms and hardware to maximize photon-capture efficiency (Kim et al., 2017).

Another important consideration is related to the type of cell that is used as the sensing element. Although microbial cells are usually robust and their integration into portable analytical devices is streamlined, they provide information that is less predictive of the effects on humans. Therefore, especially for toxicological studies, the use of mammalian cell lines is more advantageous. Interesting results were obtained with a cell biosensor smartphone platform for inflammation based on human embryonic kidney (HEK293T) cell lines genetically engineered to express the NanoLuc luciferase (Cevenini et al., 2016a). This platform provided adequate analytical performance; although, it lacked an internal viability control to correct the analytical signal according to cell toxicity. An external viability control was obtained by inclusion of wells containing cells engineered with a constitutive luciferase. This enabled parallel evaluation of nonspecific signal decays due to cell toxicity; however, an increase in signal variability due to cell-to-cell response variations was observed.

Moreover, to obtain more valuable information, e.g., in terms of the reliability of toxicity and bioactivity data, 3D cells can be developed to provide an environment that faithfully mimics the more structured in vivo physiological conditions (Dubiak-Szepietowska et al., 2016; Wittig et al., 2013). Several biosensors and prototypes were developed based on 3D multicellular cultures (spheroids), mainly relying on impedance measurements (Kloss et al., 2008; Lundstrom, 2017). The 3D cell culture systems that have been proposed to obtain spheroids that mimic the in vivo cellular microenvironment include the use of low-capacity plates, "hanging drop" systems, and rotary cell cultures (Choi et al., 2015). While all of these approaches have been optimized to obtain 3D cell cultures, their implementation into portable devices is not trivial.

Here, we report a smartphone-based platform, for quantitative effect-based analysis of analytes and complex samples having pro- or anti-inflammatory activity, relying on multicolor bioluminescent 3D cell biosensors. To the best of our knowledge, this is the first report of BL spheroid-based biosensing. We successfully applied this technology to evaluate inflammatory response induced by stressors via the NF-kB signal transduction pathway, which is induced by several types of stressors and is involved in the regulation of cell-cycle/growth, inflammation, apoptosis, and immunity (Inoue et al., 2007). Therefore, we developed and characterized a smartphone-based multicolor bioluminescent biosensor for inflammatory activity exploiting powerful red- and green-emitting luciferases. We selected luciferases with suitable emission properties for efficient spectral resolution exploiting the Bayer filter mosaic of smartphones.

The biosensor consists of immobilized spheroids of human cell lines engineered with a NFkB reporter plasmid driving the expression of a red-emitting luciferase and a second plasmid harboring a constitutively expressed green-emitting luciferase as a viability control (Fig. 1). We envisage potential applications of such an assay in different settings, such as the point-of-need analysis of environmental and food safety controls, evaluation of nutraceutical properties, and security applications for rapid monitoring of potentially harmful contaminants.

2. Experimental section

2.1. Chemical and reagents

Human embryonic kidney HEK293 cells were from ATCC (American Type Culture Collection [ATCC], Manassas, VA, USA) and cell culture reagents and materials were from Carlo Erba Reagents (Cornaredo, Milano, Italy). The enzymes required for cloning procedures were from Fermentas (Vilnius, Lithuania). The kits for plasmid extraction, beetle luciferin potassium salt (D-luciferin), and BrightGlo substrate were from Promega (Madison, WI, USA). Tumor Necrosis Factor-α (TNFα, purity higher than 95%), phorbol myristate acetate (PMA), poly(2-hydroxyethyl methacrylate) (poly-HEMA), gelatin from porcine skin type A, L-15 Medium (Leibovitz), isoproturon, naphthalene, aclonifen, hydrogen peroxide, and all other chemicals were purchased from Sigma-Aldrich (St. Louis, MO, USA). Polydimethylsiloxane (PDMS) Silgard 184 pre-polymer and curing agent were from Dow Corning (Midland, MI).

The mammalian expression plasmids pGL4.32_NFkB_Luc2P and pGL4.74[hRluc/TK] carrying Luc2P luciferase under the regulation of NFkB transcriptional regulation and hRLuc under Herpes simplex virus thymidine kinase promoter (TK) were from Promega. Plasmids PpyGR-TS and red-emitting mutant PpyRE-TS luciferase genes were previously described (Branchini et al., 2007). The reporter vectors pCMV_PpyGR-TS, pCMV_PpyRE-TS, pTK_PpyGR-TS, and pNFkB_PpyRE-TS were obtained by standard molecular cloning procedures.

2.2. 3D-printed microstructured cartridge and smartphone accessories

A cell cartridge containing 16 square wells (each 5 mm wide and 5 mm deep) was created with a desktop 3D printer (Makerbot Replicator 2 ×). The cartridge (40 × 40 mm, 7 mm height) was fabricated with black Polylactic Acid (PLA) at 210 °C, 300 μm resolution, 50% infill, printed over a customized round bottom resin film containing 500 μm microstructures with 400 μm depth, kindly provided by Elplasia™, Kuraray, Japan. Cartridges were then treated with a 30 mg/mL ethanol solution of poly-HEMA (40 μL/well) and let dry for 6 h at room temperature (25 °C) under the laminar flow hood. The cartridges were made using black PLA deposited over a microstructured sheet containing about 200 cone-shaped microspaces/cm^2 of 500 μm diameter and 400 μm depth. During the printing process, fused PLA enters into the microspaces sealing the bottom surface around each well. The 3D printed smartphone adaptors were fabricated with black acrylonitrile butadiene styrene (ABS) to provide a custom dark-box (65 × 65 mm, 60 mm high) weighting only 70 g. As the microspace film used as bottom for the cartridges is transparent, a mirror was inserted into the cartridge holder (Fig. 2e), to increase the light collected with the smartphone camera. The 3D printed parts simply snap together to form a self-supporting device (Fig. 2f). Smartphone adaptors and accessories were designed to fit the Nokia Lumia 1020 equipped with a high-performance back-side-illuminated (BSI) sensor (sensor size 1/1.5", 41MP, pixel size 1.1 μm), and printed using black ABS (at 230 °C, 300 μm resolution, 30% infill).

2.3. Bioluminescence characterization of HEK293 cells expressing green- and red-emitting luciferases with a smartphone

HEK293 cells were routinely grown in Dulbecco Modified Essential Medium (DMEM high glucose 4.5 g/L, GE Healthcare) supplemented with 10% fetal bovine serum, L-Glutamine 2 mM, 50 U/μL penicillin, and 50 μg/mL streptomycin. FuGENE HD transfection reagent (Promega) was used for transient transfections according to the manufacturer's instructions. Briefly, one day before transfection cells were plated on a 24-well plate at a density of 8 × 10^4 cells/well and transfected with 0.5 μg pCMV_PpyGR-TS or 0.5 μg pCMV_PpyRE-TS expression vector using a FuGENE®HD: DNA ratio of 3:1 and incubated at 37 °C with 5% CO_2 for 24 h. Cells were gently detached, counted, and

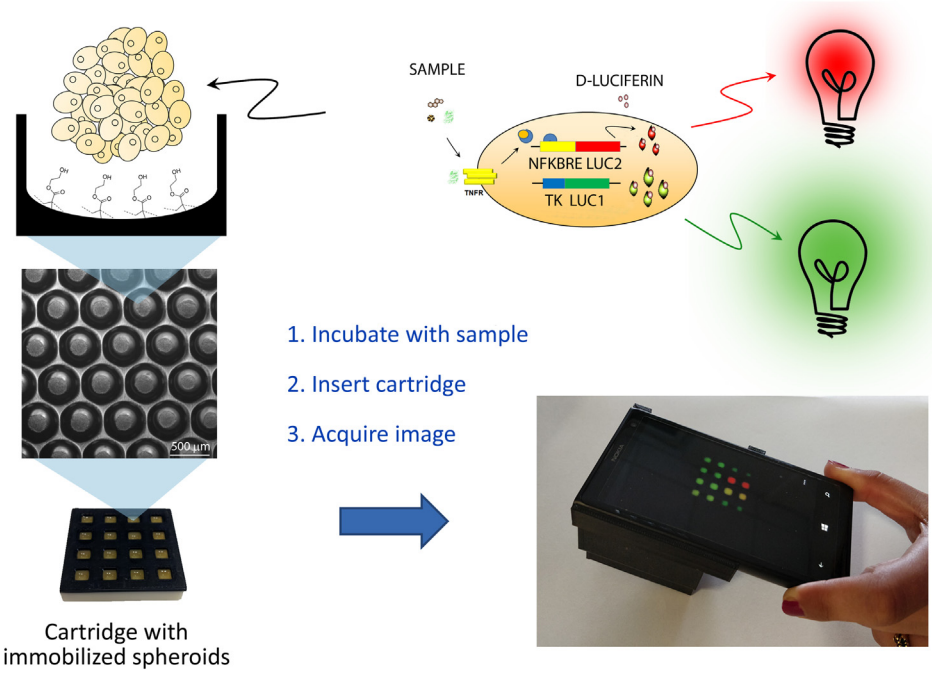

Fig. 1. Schematic representation of the genetically engineered bioluminescent cells and inflammation smartphone-based biosensor integrating dual-color bioluminescent 3D spheroids.

transferred in the 3D-printed cartridge at a density of 4.5×10^4 cells/well. Red- and green-emitting cells were diluted to a similar level of activity and imaged with the smartphone camera for 4 s using different sensitivity settings, from ISO 100 to ISO 4000, after addition of 50 µL BrightGlo substrate. The BL emission spectra (450–750 nm) and kinetics (5 min, 300 ms integration time) were acquired in a 96-well plate with a Varioskan Flash multimode reader (Thermo Fisher Scientific).

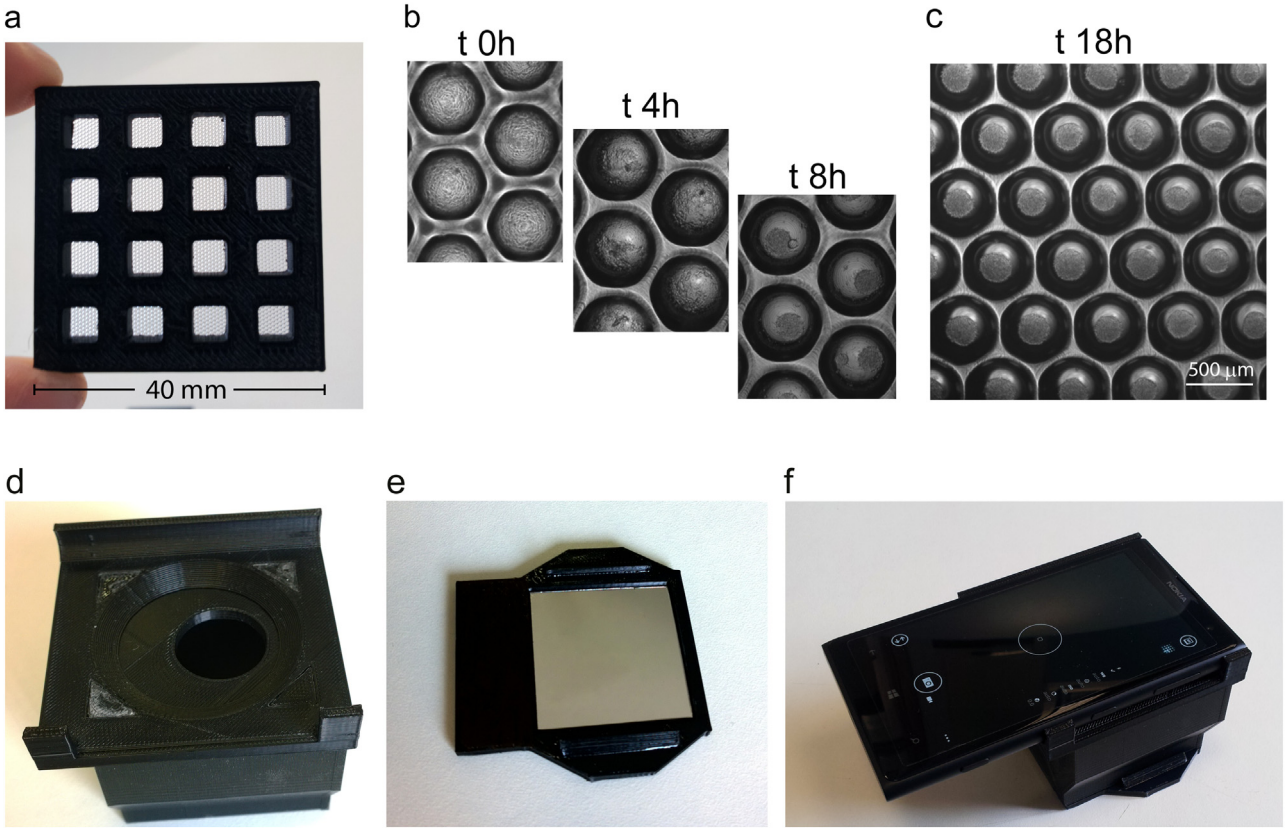

Fig. 2. 3D-printed smartphone accessories and spheroid formation; (a) Picture of the 3D printed cartridge made of PLA printed over a microspace bottom sheet; (b) HEK293-cells seeded into the cell cartridge and imaged at time 0 or after 4 h, 8 h, and 18 h overnight incubation (c); (d) Smartphone black-box accessory; (e) 3D printed cartridge holder comprising a mirror; (f) assembled smartphone-based device.

2.4. Preparation of a ready-to-use cartridge with immobilized spheroids

To develop a spheroid-biosensing platform for on-site analysis, we adopted several strategies to render the biosensor more simple and robust. A transparent PDMS lid was created using a monomer: curing agent ratio of 10:1. The solution was placed under vacuum for 40 min to remove bubbles and casted onto a 3D-printed master mold (replicating the cell-cartridge) to create the array of caps (5 ×5 mm, 2 mm height, each) that corresponded with the cell-cartridge wells. The PDMS was allowed to harden overnight at 50 °C, then gently removed from the mask and sprayed with 70% ethanol for disinfection. The spheroid biosensors were obtained by transfecting HEK293 cells with 0.1 μg pTK_PpyGR-TS and 0.4 μg pNFkB_PpyRE-TS in 24-well plates and were transferred (4.5×10^4 cells/well) into the 3D printed cell cartridge to enable spheroid formation. After overnight incubation at 37 °C, a 50 μL-volume of 5% w/v gelatin solution (in complete medium) was added to each well. The cell-cartridge was kept at room temperature (25 °C) to allow the gelatin to set and form a gel in the wells, then sealed with the PDMS lid. To control spheroid formation and optimize the protocol, spheroids were imaged with an inverted microscope (Olympus IX73) using a 4X objective (Olympus UPlanFLN).

Spheroid analysis was performed from bright-field images of HEK293 spheroids using ImageJ version 1.51d software to define for each spheroid's perimeter (P) and projected area (A). We calculated a sphericity factor Φ (Kelm et al., 2003) as follows:

$$\phi = \frac{\pi \sqrt[x]{\frac{4A}{\pi}}}{P} \quad (1)$$

2.5. Development of a smartphone-based dual-color inflammation spheroid biosensor

Different parameters were optimized in order to improve the 3D cell biosensor analytical performance in terms of selectivity, analysis time, and robustness. Thus, we changed different parameters including the choice of promoters, transfection ratio between different reporter plasmids, cell density at seeding (1.5×10^4, 3×10^4, and 4.5×10^4), and incubation time for achieving efficient and reproducible formation of spheroids (from 4 to 18 h). Briefly, under optimized conditions, HEK293 cells were transiently transfected in 24-well plates with 0.1 μg pTK_PpyGR-TS, for the constitutive expression of a green-emitting luciferase used as the viability control, and with 0.4 μg pNFkB_PpyRE-TS, a reporter vector in which a red-emitting luciferase is under the control of NFkB response elements (Fig. 1). At 24 h post-transfection, 40 μL of cells resuspended in DMEM (4.5×10^4 cells/well) were transferred into the 3D-printed cell cartridge and incubated at 37 °C for spheroid formation. After 18 h, a cartridge containing spheroids was treated in duplicate with 10 μL TNFα dilutions (concentration range 0.5–20 ng/mL from a stock solution of 10 μg/mL TNFα in phosphate-buffered saline solution) or culture medium, as a control (blank). After 5 h incubation, a 50 μL-volume of BrightGlo substrate was added to each well and BL images were acquired with the smartphone (4 s, ISO 800) assembled with the 3D printed accessories.

Images were analysed with ImageJ software (National Institutes of Health, Bethesda, MD) and GraphPad Prism v.5 (GraphPad Software, La Jolla, USA) was used to plot the data. Briefly, each image was split into RGB channels and the emission of PpyGR-TS and PpyRE-TS were quantified by selecting regions of interest (ROIs) on corresponding images to calculate the mean integrated density of duplicate wells. The dose-response curve for TNFα was obtained by calculating the red to green emission ratio for each concentration (corrected BL signals) and by plotting these values as fold response with respect to control (CTR). Limit of Detection (LOD) was calculated as the TNFα concentration that corresponds to the blank plus three times the standard deviation. All measurements were performed in duplicate and repeated with different cell cartridges at least three times.

2.6. Selectivity of the biosensor

To evaluate the selectivity of the inflammation spheroid biosensor we tested different chemicals including pollutants and pesticides, i.e., isoproturon, aclonifen and naphthalene regulated by the European Union (Water Framework Directive 2000/60/EC) and World Health Organization. The maximum allowable concentration Environmental Quality Standards (MAC-EQS) admitted by Directive 2013/39/EU in inland surface waters were tested: 0.12 μg/L for aclonifen, 130 μg/L for naphthalene and 1.0 μg/L for isoproturon. Mixture solutions of different chemicals were analysed to assess additive or synergic effects of the compounds on the NFkB inflammation pathway. Four different mixtures were analysed: Mix 1 (isoproturon 1.0 μg/L + naphthalene 130 μg/L), Mix 2 (isoproturon 1.0 μg/L and aclonifen 0.12 μg/L), Mix 3 (aclonifen 0.12 μg/L and naphthalene 130 μg/L), Mix 4 (aclonifen 0.12 μg/L, naphthalene 130 μg/L and isoproturon 1.0 μg/L). To investigate the specific effects of reactive oxygen species (ROS) spheroid cartridges were treated with H_2O_2 solutions (concentration range from 0.5 mM to 10 mM in doubly distilled water).

Spheroid cartridges were treated in duplicate with 10 μL solutions of pure chemicals or mixtures 1–4. Cells transfected only with pNFkB_PpyRE-TS and induced with 10 ng/mL TNFα were also prepared as the inflammatory positive control; while doubly distilled water was used as the negative control. After 5 h incubation, a 50 μL volume of BrightGlo substrate was added to each well and BL images were acquired with the smartphone (4 s, ISO 800) and analysed as previously described with ImageJ.

2.7. Simulation of real samples

We investigated the suitability of the 3D spheroid biosensor to analyze samples with pro-inflammatory activity or general toxicity, thus being potentially harmful to human health. The chemical agent chosen for inflammation monitoring was PMA, a phorbol ester isolated from *Jatropa Curcas*, a plant widely used as biodiesel feedstock that contains pro-inflammatory phorbol esters (EFSA CONTAM Panel, 2015).

Spheroid cartridges were treated in duplicate with 10 μL PMA solutions ranging from 0.1 nM to 10 μM in 5% DMSO. Cells transfected only with pNFkB_PpyRE-TS and induced with 10 ng/mL TNFα were also prepared as the inflammatory positive control; while, DMSO, 1% final concentration, was used as the negative control. After 5 h incubation, a 50 μL volume of BrightGlo substrate was added to each well and BL images were acquired with the smartphone (4 s, ISO 800) and analysed as previously described with ImageJ. In order to obtain a robust biosensor and a reproducible assay for on-site applications, the analytical performances of spheroid cartridges were also evaluated after one week storage. Cell-cartridges with immobilized spheroids in L-15 Medium (Leibovitz) were maintained at room temperature (25 °C) for up to one week before assay execution. All measurements were repeated with 3 different cartridges.

3. Results and discussion

The possibility to use the smartphone camera to detect bio/chemiluminescent reactions has been previously reported (Roda et al., 2014b; Cevenini et al., 2016b; Kim et al., 2017). However, the full exploitation of a smartphone-integrated CMOS camera to simultaneously detect multiple colors emitted by genetically engineered cells in the same well has not been reported yet. In addition, the implementation of 3D cell cultures, i.e. spheroids, for smartphone-based biosensing has not been addressed.

The proposed biosensing platform for on-site analysis required adaptation to preserve the functionality of the cells while maintaining

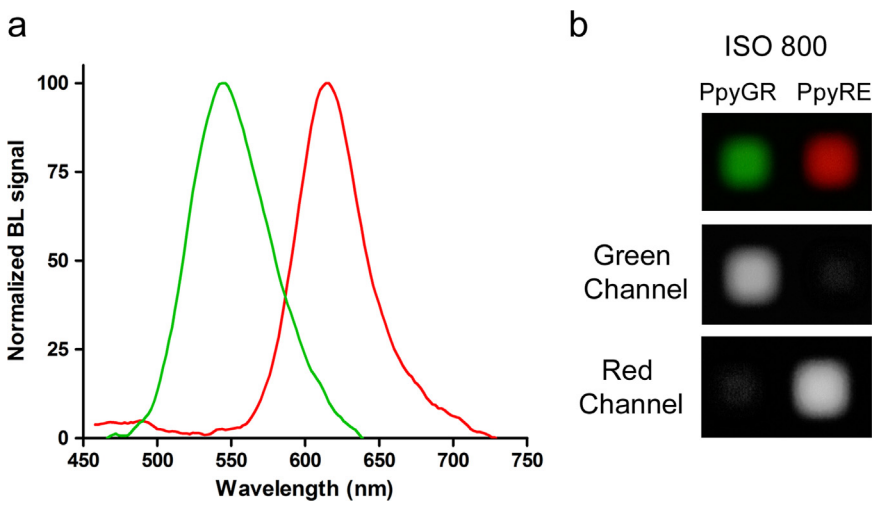

Fig. 3. (a) BL emission spectra of HEK293-spheroids expressing green (PpyGR-TS) and red-emitting (PpyRE-TS) thermostable luciferase mutants obtained with Varioskan Flash luminometer; (b) Color image of green and red-emitting luciferases in HEK293-spheroids acquired with the smartphone for 4 s at ISO 800 and same image split into green and red channels to evaluate the crosstalk between PpyGR-TS and PpyRE-TS emission.

adequate sensitivity. In fact, although spheroid-biosensors have been reported (Wittig et al., 2013), integration within a biosensor device has not been effectively demonstrated. Prompted by proof-of-principle biosensors and cell-based assays relying on 3D cell cultures (Cevenini et al., 2017; Dubiak-Szepietowska . et al., 2016), we developed a new 3D cell format in which spheroids are immobilized into a 3D cartridge that plugs into a smartphone. Here, we report a dual-color BL spheroid-biosensor platform, in which a red-emitting luciferase is induced by the presence of pro-inflammatory stimuli and a green-emitting reporter is constitutively expressed and used as a viability control. The presence of inflammatory compounds in the sample will increase the red BL signal and the independent viability green signal will allow us to correct the response for nonspecific effects or general toxicity activity. Thus, this dual sensor will distinguish between pro-inflammatory agents and chemicals having general cell toxicity.

3.1. Fabrication of 3D cell-culture cartridges and smartphone accessories

As shown in Fig. 2a, we developed a customized 3D-printed cartridge (40 × 40 mm) containing 16 square wells (5 mm wide and 5 mm deep). The cartridge was printed with black PLA over a resin film containing 500 μm microstructures with 400 μm depth. We could not opt for ABS as the printing material, although its feasibility for integrating bioluminescent cell biosensors was recently reported (Cevenini et al., 2016a, 2016b), because it requires a heating bed. Heat beds are commonly used in 3D printing to avoid warping and improve print quality; however, the temperatures used for ABS (100–110 °C) would destroy the cone-shaped microstructures (about 200 cones per cm^2). Therefore, we used black PLA, which does not require a heated bed and preserves the microstructures.

The cartridge surface was then treated with poly-HEMA to facilitate cell-cell rather than cell-plastic interactions, thus promoting cell aggregation into spheroids. Poly-HEMA hydrogels are polymers approved by federal agencies for the use in several biomedical and pharmaceutical applications. The non-toxicity and the biocompatibility of the poly-HEMA makes it suitable for most biotechnological applications. Moreover, thanks to the presence of polar groups and hydrophobic α-methyl groups, the polymer has excellent chemical properties in terms of mechanical strength stability and compatibility with water (Kim et al., 2015).

HEK293 were selected to provide endogenous expression of TNFα receptor, a potent mediator of inflammation, as they aggregate very quickly and form spheroids within a few hours (Fig. 2b, c). After an overnight incubation, HEK293 spheroids of 190 ± 20 μm were formed. The sphericity factor (ϕ) of 20 spheroids was calculated according to Eq. (1) obtaining an average value of 0.93 ± 0.02, which is consistent with that obtained in commercial 96-well micropatterned plates (Cevenini et al., 2017). This cartridge configuration provides 16 wells, each containing approximately 50 spheroids, thus providing a ready-to-use platform that can be snapped into the smartphone and imaged.

3.2. Bioluminescence characterization of red and green-emitting 3D spheroids with the smartphone

To fully exploit the possibilities offered by the color BI-CMOS camera of smartphones, we set up a dual-color biosensor based on the expression of two luciferases emitting at different wavelengths. The implementation of dual-color imaging represents a significant upgrade in smartphone-based devices (Wang et al., 2017); nevertheless, the implementation of low-light emitting probes, such as bioluminescent reporters, challenges the sensitivity of the smartphone integrated camera. Therefore we selected two highly stable mutant luciferases, PpyGR-TS and PpyRE-TS luciferases that showed advantageous properties, i.e., high emission intensity, glow-type kinetics (Branchini et al., 2007), and high pH stability, as the viability control and inflammation reporter, respectively. These thermostable human codon optimized luciferases (Fig. 3a), with emission maxima at 549 nm and 615 nm and corresponding bandwidths at half maxima of 70 nm and 50 nm, respectively, provide well separated emission spectra using the same D-luciferin substrate. These optimal spectral features enable the analysis of complex matrices. Thus, the assay is highly cost effective. In addition, the BL emission spectra of these luciferases nearly overlap the spectral transmittance of the green and red filters of the Bayer matrix in the smartphone CMOS sensor, allowing sensitive detection of BL signals.

In this work, we took advantage of the smartphone Nokia Lumia 1020, which is equipped with a camera with built-in ProCam application enabling manual selection of different parameters. In particular, the possibility to set the shutter speed up to 4 s and to use ISO values up to 4000, makes this smartphone suitable for low-light imaging applications. To optimize the acquisition of BL signals, we imaged HEK293 spheroids expressing the green- or red-emitting luciferase, using different exposure times and ISO values from 100 to 4000. Use of a low exposure time (i.e. 1 or 2 s) in combination with high ISO values, resulted in noisy images (data not shown). At ISO 800, about 95% of green luciferase emission is acquired in the green channel and only a 5% is detected in the red channel (and vice versa) (Fig. 3b). The crosstalk between channels increases with higher sensitivity settings and the signal to background ratio is not significantly improved (less than 8%). At ISO 1600, a significant interference was observed, with about 25% of PpyGR-TS emission detected in the red channel and 15% of PpyRE-TS acquired in the green channel. For this reason, for the

quantification of the spheroid-biosensor response, we acquired BL images for 4 s at ISO 800 to achieve the best sensitivity and lowest crosstalk between the two luciferases.

3.3. Optimization and analytical performance of smartphone-based dual-color inflammation biosensor

It is recognized that 3D cell cultures are stable for longer lifespans than 2D cell cultures and provide more suitable tools to develop cell biosensors with adequate responsiveness over time. For example, Bhise et al. reported that bioprinted hepatic spheroids remained functional during a 30 day culture period (Bhise et al., 2016). However, the reported liver-on-a-chip platform, used for toxicity assessment, required continuous perfusion and cannot be implemented into a low-cost platform. Moreover, another issue to be considered is related to the limited diffusional transport posed by the 3D structure of the spheroids. Multicellular aggregates are composed of proliferating cells, non-proliferating viable cells, and necrotic cells. The presence of multiple phenotypes mimics the in vivo tumor physiology and may represent an advantage in cancer research (Jeong et al., 2012). However, this could represent a caveat in biosensing with bioluminescent reporters due to the limited availability of the analytes and substrates for the chemical reaction, as well as oxygen, which is required for all luciferase-based reactions. In spheroids with a diameter of 150 μm, the majority of cells have sufficient oxygen for BL reactions, with a negligible necrotic core composed of only 2% of cells (Langan et al., 2016). Therefore, we decided to obtain spheroids in the range of 150–200 μm.

In order to obtain a stand-alone spheroid-based biosensing platform for on-site analysis, we integrated the spheroid-biosensors in a ready-to-use 3D printed cartridge. To this end, BL spheroid biosensors were immobilized with a medium solution containing 5% v/v gelatin from porcine skin type A. It has been reported that the inclusion of gelatin microparticles increases the stiffness of the spheroid microenvironment (Baraniak et al., 2012), enabling quick and easy interaction with the sample (and the availability of the chemical substrate for the BL reaction).

We aimed at obtaining color-coded visual information in which the green emission is associated with “safe”; while, the red corresponds to “harmful” samples. Since the green luciferase is constitutively expressed, the presence of compounds able to activate the intracellular inflammatory pathway will produce a yellowish to orange color proportional to induction levels and to general toxicity effects. Obtaining a color emission which covers a wide range of green to red hues, largely depends on the relative expression of the two luciferases. This can be tuned by adjusting the promoter strength and the ratio between the two reporter plasmids used for cell transfection. We first expressed the green luciferase under the strong CMV promoter (pCMV_PpyGR-TS). When incubating HEK293 co-transfected with pNFkB_PpyRE-TS and pCMV_PpyGR-TS with TNFα concentrations in the range 0.5–20 ng/mL, the signal of constitutive green-emitting luciferase was too high, overlapping the red channel. It was not possible to perform spectral resolution to quantitatively elaborate the corrected inflammatory response (data not shown). Therefore, to reduce the expression level of PpyGR-TS, the weaker Herpes simplex virus thymidine kinase promoter was selected (Qin et al., 2010). We then optimized the transfection protocols to achieve the optimum balance between red and green emission. Cells were transfected with a 1:1 and 1:3 ratio of pTK_PpyGR-TS and pNFkB_PpyRE-TS vectors. Using the same amount of reporter plasmids, the LOD for TNFα was 20 ng/mL, limiting the applicability of the assay. Therefore, a ratio of 1:3 control: reporter vector was selected, providing the full range of “traffic light” emissions. Fig. 4a shows a typical image obtained with the smartphone by incubating the spheroid-biosensor with increasing concentrations of TNFα. Spheroids expressing only PpyRE-TS induced with 20 ng/mL TNFα and spheroids incubated with vehicle only are also present in each cartridge as positive and negative inflammatory controls, respectively.

Multicolor cell-based assays performed with conventional instrumentation (i.e. luminometer) usually relies on the use of optical emission filters to acquire the BL signals from luciferases emitting at different wavelength and on a spectral unmixing algorithm for the separation of emitted light. Despite the spectral overlap between the two luciferases, the low crosstalk between channels (5%) allows the user to simply quantify the BL emission of PpyGR-TS and PpyRE-TS on green- and red-channel split images (Fig. 4b), respectively. The BL signal of both luciferases in the blue channel is negligible (less than 1%) and is excluded from calculations. The BL signal of green- and red-emitting luciferases were quantified on corresponding images, by selecting a square ROI around each well, and plotted as the mean ± SD of duplicate wells. A mirror was also placed under the cartridge to increase the acquisition of BL emission. Back-reflection towards the CMOS sensor through the transparent gelatin layer provided an increase of about 40% in the light collected.

The calibration curve for TNFα was obtained by calculating the corrected BL signal (PpyRE-TS/PpyGR-TS emission ratio) for each concentration and by plotting the corresponding fold response with respect to the control (CTR) (Fig. 4c). The ratiometric measurement provides a more robust analysis since aspecific effects on cell viability as well as small variations in spheroid number and dimension are corrected. In optimized conditions, i.e. a cartridge with 50 spheroids/well transfected at a 1:3 viability: inflammatory reporter vector ratio, 5 h incubation, and acquisition for 4 s (ISO 800), the smartphone-based biosensor provides a LOD of 0.15 ± 0.05 ng/mL and an EC50 of 1.0 ± 0.1 ng/mL TNFα. Indeed, reporter-gene assays were suitable for the high throughput quantification of residual drug activity and anti-drug neutralizing antibody response to TNFα antagonists in serum samples (Lallemand et al., 2011). Therefore, a potential application could be as point-of-care diagnostics for patients with inflammatory disease, such as Crohn's disease, treated with a TNFα antagonist.

3.4. Selectivity of the biosensor

To assess the selectivity of the biosensor we evaluated the inflammatory activity and toxicity of different toxic chemicals having dissimilar modes of action and classified as priority substances or pollutants by the European Union (EU) and the United States Environmental Protection Agency (EPA). We analysed the activity of these compounds at the Maximum Allowable Concentration for inland surface waters defined in the Environmental Quality Standards (MAC-EQS) of Directive 2013/39/EU. We selected isoproturon, an agricultural herbicide of low acute toxicity and medium toxicity after short- and long-term exposures, which has been detected in surface and ground water at concentrations below 0.1 μg/L (WHO, 2003). We also analysed aclonifen, a biocide causing oxidative damage via the formation of reactive oxygen species (ROS) (Almeida et al., 2017) and naphthalene, whose exposure has been associated with hemolytic anemia and damage to the liver, which has been classified as a possible human carcinogen by EPA (Höke and Zellerhoff, 1998). As expected, at the tested concentrations, i.e., 0.12 μg/L for aclonifen, 130 μg/L for naphthalene and 1.0 μg/L for isoproturon, these compounds did not produce any activation of the NF-κB pathway and did not show significant cell toxicity. Pollutants, and in particular pesticides, may occur at low concentrations in mixtures with other chemicals (Hernández et al., 2013). Therefore, from a toxicological perspective, it is of paramount importance to assess the overall activity of a sample (Busch et al., 2016). Since a potential application of the proposed biosensor is the evaluation of total toxicity of an environmental sample to rapidly identify potential threats to human and animal health, we also analysed mixtures of these compounds which could be present in inland surface waters, encompassing rivers, lakes, and artificial water bodies. Interestingly, the mixtures Mix 3 (aclonifen 0.12 μg/L and naphthalene 130 μg/L) and Mix 4 (aclonifen 0.12 μg/L, naphthalene 130 μg/L, and isoproturon 1 μg/L) presented significant toxic effects with a drop in

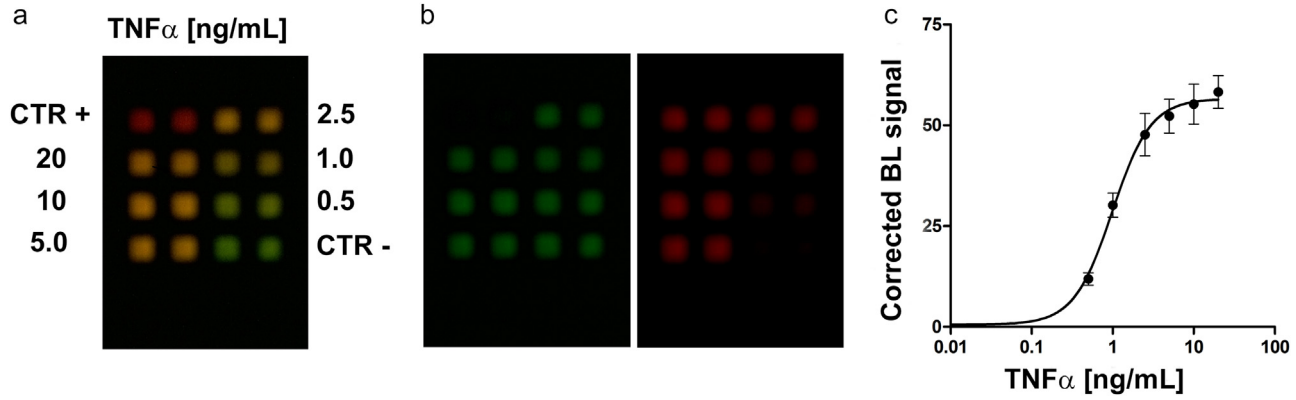

Fig. 4. (a) Image acquired with the smartphone obtained by incubating the spheroid-biosensor with increasing concentrations of TNFα; (b) Green- and red-channel images corresponding to the PpyGR-TS (viability signal) and PpyRE-TS (inflammatory response) emission; (c) corrected dose-response curve for TNFα.

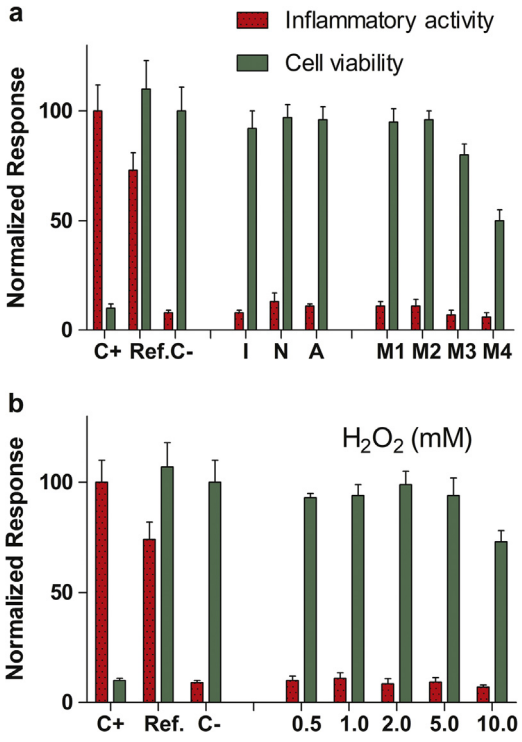

Fig. 5. (a) Results obtained by incubating the 3D cell biosensor with chemicals for 5 h at room temperature (25 °C) and imaged with the smartphone. Positive inflammatory control C+ : 10 ng/mL TNFα; Ref.: 2.5 ng/mL TNFα, Viability control Ctr-: doubly distilled water; I: isoproturon 1.0 μg/L; N: naphthalene 130 μg/L; A: aclonifen 0.12 μg/L; M1: mixture solution containing isoproturon 1.0 μg/L and naphthalene 130 mg/L; M2: mixture solution containing isoproturon 1 mg/L and aclonifen 0.12 mg/L; M3: mixture solution containing aclonifen 0.12 mg/L and naphthalene 130 mg/L; M4: mixture solution containing aclonifen 0.12 mg/L, naphthalene 130 mg/L and isoproturon 1 mg/L). (b) Results obtained with 5 h incubation at 25 °C of the 3D biosensor with different concentrations of H_2O_2 (concentration range 0.5–10 mM). Cell viability was normalized with respect to the green emission of control wells, while inflammatory activity was reported as the fold induction of the red-calibrator emission. Values are the mean ± standard deviations of three experiments performed in duplicate.

cell viability of 20 ± 5% and 51 ± 8%, respectively (Fig. 5a).

3.5. Simulation of real sample analysis

As proof of concept, the response of the dual-color biosensor was tested using spiked samples containing different concentration of PMA, a NF-kB activator that is used in pharmacology as a potent tumor promoter and for activating protein kinase C (Lee et al., 2002). PMA is extracted from the *Jatropha curcas* plant, which gained importance in recent years as it grows in different soil conditions and its seeds are a source of oil for biofuel production (EFSA CONTAM Panel, 2015). The by-product called Jatropha meal has a high nutritional value and may be used as a feed ingredient for the animal industry. However, due to the presence of phorbol esters, well-known toxicants having tumor promoting activity, detoxification treatments are necessary prior to its use in animal feed. PMA in fact induces malignant transformation of cells via the activation of c-Jun and c-Fos. The subsequent proinflammatory response to tumor promotion is then mediated through activation of NF-κB (Goel et al., 2007). A simple biosensing platform might be useful for the evaluation of treatment efficacy and to monitor the phorbol esters content in Jatropha derived products or possible contamination in the environment (e.g. water).

To create a user-friendly platform, each cartridge also provides a traffic light like response as a reference for a quick evaluation of the sample's activity. This was obtained by including i) spheroids transfected with reporter vector only and induced with 10 ng/mL TNFα, which provide a red emission (positive control, Ctr+), ii) spheroids transfected with both reporter and control vectors and induced with 2.5 ng/mL TNFα, which provide a yellow-orange emission, and iii) spheroids transfected with both reporter and control vectors and incubated with vehicle (DMSO 1%), resulting in green-emission only (negative control, Ctr-) (Fig. 6).

By testing the same concentration of PMA (10 nM) the response of the biosensor was reproducible with an intra-assay variability of 13% and an inter-assay variability of 17%, the latter obtained with different cartridges.

It is known that inflammatory pathways and cellular oxidative stress are interconnected and reactive oxygen intermediates (e.g., H_2O_2) act as NF-κB inducers (Legrand-Poels et al., 1995). Therefore, to better understand if PMA effects were due to pure NF-κB activation or mediated by cellular oxidative stress, we investigated the effect of H_2O_2 on the biosensor. As shown in Fig. 5b, only at a concentration of 10 mM was H_2O_2 able to decrease cell viability (27 ± 5%) within the 5 h of incubation. None of the tested H_2O_2 concentrations (range 0.5–10 mM) produced pro-inflammatory effects (Fig. 5b).

We evaluated the possibility to store cartridges at room temperature (25 °C) for one week. To this end we replaced DMEM with L15 medium, which is formulated for use in carbon dioxide free systems. In a previous work, ready-to-use cartridges with immobilized HEK293 cells showed a 40 ± 7% drop in bioluminescence after 48 h at 25 °C storage (Cevenini et al., 2016a). Such loss in viability caused a non-reliable response after 2 days storage of the cartridge. On the other hand, spheroids showed a much slower decrease in viability (20 ± 8% drop in bioluminescence after one week storage at room temperature),

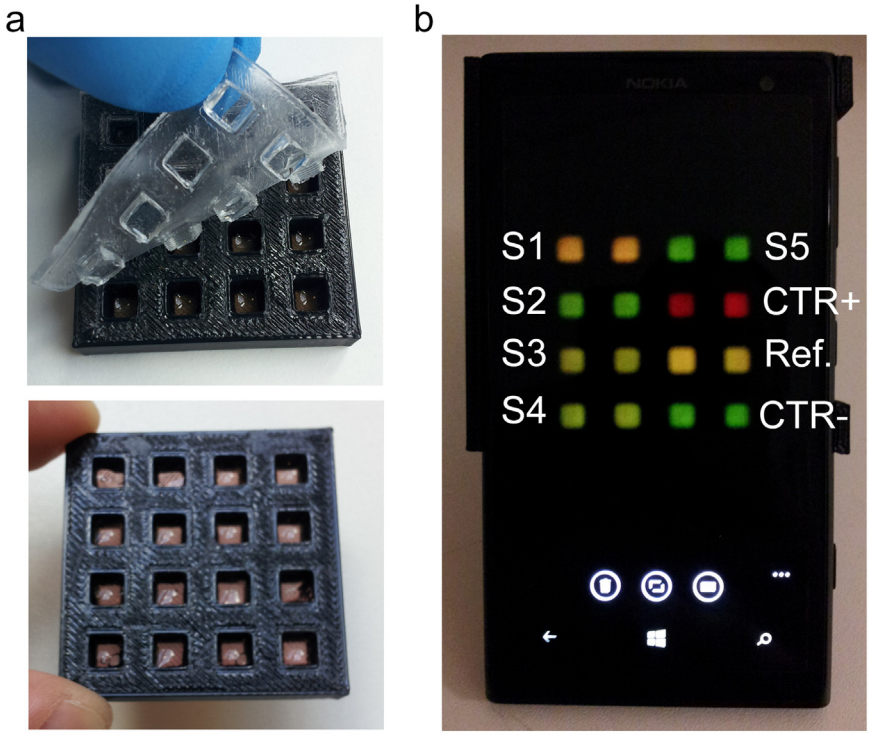

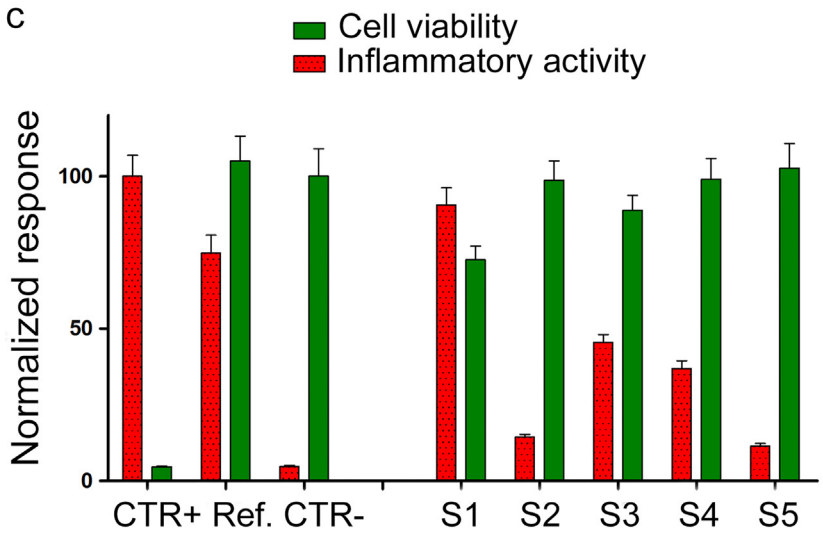

Fig. 6. (a) Picture of the 3D printed cartridge containing the immobilized spheroid-biosensor. Each cartridge can be used to analyze up to five samples in duplicate. It contains a positive control (Ctr+), a reference, and a negative control (Ctr-) resulting in a sort of "traffic light" response for direct comparison of the sample's activity; (b) BL image, obtained with the smartphone, of a cell cartridge incubated with different concentrations of PMA: S1 (10 μM PMA), S2 (1 nM PMA), S3 (1 μM PMA), S4 (50 nM PMA), S5 (0.1 nM PMA), Ctr+ (10 ng/mL TNFα), Ref. (2.5 ng/mL TNFα), Ctr- (1% DMSO); (c) Results obtained after image elaboration of the tested samples. Cell viability was normalized with respect to the green emission of control wells, while inflammatory activity was reported as the fold induction of the red-calibrator emission.

which, in conjunction with the use of internal correction, provided a correct evaluation of inflammatory activity of the samples even after seven days. For example sample S3 containing 1 μM PMA showed corrected inflammatory activities of 49% and 47% compared to Ctr + (10 ng/mL TNFα), at day 0 and after 7 days of storage, respectively (corresponding viabilities were 91 ± 8% and 75 ± 8%).

As expected, an higher variability between duplicates was reported (CV%= 20%) after one week storage, however, due to their higher stability, spheroids provided a significant improvement in the cells' shelf-life when compared to cells immobilized in conventional matrices. These pre-loaded cartridges could be shipped or transported with commercially available portable incubators directly to the site were the analysis is required. This greatly simplifies the transport and use of our biosensor in laboratories non equipped with cell-culture facilities (e.g., cell culture incubators with CO_2 controlled atmosphere) and benchtop instrumentation for bioluminescence detection.

4. Conclusion

We implemented a multicolor bioluminescent 3D cell biosensor in a smartphone-based platform. The biosensor consists of immobilized spheroids of human cell lines expressing red- and green light emitting luciferase under the regulation of the NFkB pathway and a constitutive promoter, respectively. The 3D cell biosensor enables the assessment of the actual toxicity and inflammatory effects of a sample, rather than identifying single constituents. Such a biosensor could be thus very helpful in those situations in which mixtures of compounds with unknown toxicities and different mode of action are present, such as the aquatic environment. From this perspective, the proposed biosensing platform would aim to become a useful tool for an initial screening of environmental samples or toxic substances on-site, thus identifying samples for a more accurate chemical analysis. However, it must be pointed out that 3D cell models still do not compete with the robustness of microbial biosensors based on bacterial or yeast cells and future work

will regard the development of new immobilization matrices to improve the shelf-life of 3D cell models. Moreover, spheroids obtained from different engineered cell lines could be obtained to enlarge the spectrum of target bioactivities, including liver toxicity, genotoxicity, and oxidative stress response.

Acknowledgments

This research was sponsored in part by the NATO Science for Peace and Security Programme under Grant No. 985042, by Italian Ministry of Education under grants PRIN 2015 (Prot. 2015TWP83Z) and PRIN2015 (Prot. 2015FFY97L), and LAV.

Conflict of interests

The authors declare no competing financial interest.

References

Almeida, A.C., Gomes, T., Langford, K., Thomas, K.V., Tollefsen, K.E., 2017. Aquat. Toxicol. 189, 50–59.
Arts, R., den Hartog, I., Zijlema, S.E., Thijssen, V., van der Beelen, S.H., Merkx, M., 2016. Anal. Chem. 88, 4525–4532.
Baraniak, P.R., Cooke, M.T., Saeed, R., Kinney, M.A., Fridley, K.M., McDevitt, T.C., 2012. J. Mech. Behav. Biomed. Mater. 1, 63–71.
Bazin, I., Seo, H.B., Suehs, C.M., Ramuz, M., De Waard, M., Gu, M.B., 2017. Environ. Sci. Pollut. Res. Int. 24, 33–41.
Bhise, N.S., Manoharan, V., Massa, S., Tamayol, A., Ghaderi, M., Miscuglio, M., Lang, Q., Shrike Zhang, Y., Shin, S.R., Calzone, G., Annabi, N., Shupe, T.D., Bishop, C.E., Atala, A., Dokmeci, M.R., Khademhosseini, A., 2016. Biofabrication 81, 014101.
Branchini, B.R., Ablamsky, D.M., Murtiashaw, M.H., Uzasci, L., Fraga, H., Southworth, T.L., 2007. Anal. Biochem. 361, 253–262.
Busch, W., Schmidt, S., Kühne, R., Schulze, T., Krauss, M., Altenburger, R., 2016. Environ. Toxicol. Chem. 35, 1887–1899.
Cevenini, L., Calabretta, M.M., Lopreside, A., Branchini, B.R., Southworth, T.L., Michelini, E., Roda, A., 2017. Photochem. Photobiol. 93, 531–535.
Cevenini, L., Calabretta, M.M., Lopreside, A., Tarantino, G., Tassoni, A., Ferri, M., Roda, A., Michelini, E., 2016a. Anal. Bioanal. Chem. 408, 8859–8868.
Cevenini, L., Calabretta, M.M., Tarantino, G., Michelini, E., Roda, A., 2016b. Sens. Actuators B: Chem. 225, 249–257.
Cevenini, L., Camarda, G., Michelini, E., Siciliano, G., Calabretta, M.M., Bona, R., Kumar, T.R., Cara, A., Branchini, B.R., Fidock, D.A., Roda, A., Alano, P., 2014. Anal. Chem. 86, 8814–8821.
Cevenini, L., Lopreside, A., Calabretta, M.M., D'Elia, M., Simoni, P., Michelini, E., Roda, A., 2018. Anal. Bioanal. Chem. 410, 1237–1246.
Choi, J., Lee, E.K., Choo, J., Yuh, J., Hong, J.W., 2015. Biotechnol. J. 10, 1682–1688.
Comina, G., Suska, A., Filippini, D., 2016. Biosens. Bioelectron. 77, 1153–1167.
Ding, Y., Hua, X., Chen, H., Liu, F., González-Sapien, G., Wang, M., 2018. Anal. Chem. 90, 2230–2237.
Directive 2000/60/EC of the European Parliament and of the Council of 23 October 2000 establishing a framework for Community action in the field of water policy. 〈http://ec.europa.eu/environment/water/water-framework/index_en.html〉.
Dubiak-Szepietowska, M., Karczmarczyk, A., Winckler, T., Feller, K.H., 2016. Toxicology 370, 60–69.
EFSA CONTAM Panel (EFSA Panel on Contaminants in the Food Chain), 2015. EFSA J. 13, 4321.
Elad, T., Lee, J.H., Gu, M.B., Belkin, S., 2010. Adv. Biochem. Eng. Biotechnol. 117, 85–108.
Goel, G., Makkar, H.P., Francis, G., Becker, K., 2007. Int J. Toxicol. 26, 279–288.
He, W., Yuan, S., Zhong, W.H., Siddikee, M.A., Dai, C.C., 2016. Appl. Microbiol. Biotechnol. 100, 1109–1119.
Hernández, A.F., Parrón, T., Tsatsakis, A.M., Requena, M., Alarcón, R., López-Guarnido, O., 2013. Toxicology 307, 136–145.
Höke, H., Zellerhoff, R., 1998. Toxicology 126, 1–7.
Inoue, J., Gohda, J., Akiyama, T., Semba, K., 2007. Cancer Sci. 98 (3), 268–274.
Jeong, S.H., Lee, D.W., Kim, S., Kim, J., Ku, B., 2012. Biosens. Bioelectron. 35, 128–133.
Kabessa, Y., Eyal, O., Bar-On, O., Korouma, V., Yagur-Kroll, S., Belkin, S., Agranat, A.J., 2016. Biosens. Bioelectron. 79, 784–788.
Kelm, J.M., Timmins, N.E., Brown, C.J., Fussenegger, M., Nielsen, L.K., 2003. Biotechnol. Bioeng. 83, 173–180.
Kim, H.J., Jeong, H., Lee, S.J., 2018. Anal. Bioanal. Chem. 410, 1191–1203.
Kim, H., Jung, Y., Doh, I.J., Lozano-Mahecha, R.A., Applegate, B., Bae, E., 2017. Sci. Rep. 7, 40203.
Kim, J.H., Lim, I.R., Joo, H.J., Choi, S.C., Choi, J.H., Cui, L.H., Iim, L., Hong, S.J., Lim, D.S., 2015. Biochem. Biophys. Res. Commun. 468, 372–379.
Kloss, D., Fischer, M., Rothermel, A., Simon, J.C., Robitzki, A.A., 2008. Lab Chip. 8, 879–884.
Lallemand, C., Kavrochorianou, N., Steenholdt, C., Bendtzen, K., Ainsworth, M.A., Meritet, J.F., Blanchard, B., Lebon, P., Taylor, P., Charles, P., Alzabin, S., Tovey, M.G., 2011. J. Immunol. Methods 373, 229–239.
Langan, L.M., Dodd, N.J., Owen, S.F., Purcell, W.M., Jackson, S.K., Jha, A.N., 2016. PLoS One 11, e0149492.
Lee, H.W., Ahn, D.H., Crawley, S.C., Li, J.D., Gum, J.R., Basbaum, C.B., Fan, N.Q., Szymkowski, D.E., Han, S.Y., Lee, B.H., Sleisenger, M.H., Kim, Y.S., 2002. J. Biol. Chem. 277 (32624-32624).
Legrand-Poels, S., Bours, V., Piret, B., Pflaum, M., Epe, B., Rentier, B., Piette, J., 1995. J. Biol. Chem. 270, 6925–6934.
Lundstrom, K., 2017. Expert Opin. Drug Discov. 12, 335–343.
Michelini, E., Roda, A., 2012. Anal. Bioanal. Chem. 402, 1785–1797.
Niwa, K., Ichino, Y., Kumata, S., Nakajima, Y., Hiraishi, Y., Kato, D., Viviani, V.R., Ohmiya, Y., 2010. Photochem. Photobiol. 86, 1046–1049.
Preechaburana, P., Suska, A., Filippini, D., 2014. Trends Biotechnol. 32, 351–355.
Qin, J.Y., Zhang, L., Clift, K.L., Hulur, I., Xiang, A.P., Ren, B.Z., Lahn, B.T., 2010. PLoS One 5 (5), e10611.
Raut, N., O'Connor, G., Pasini, P., Daunert, S., 2012. Anal. Bioanal. Chem. 402, 3147–3159.
Roda, A., Cevenini, L., Borg, S., Michelini, E., Calabretta, M.M., Schüler, D., 2013. Lab Chip. 13, 4881–4889.
Roda, A., Guardigli, M., Calabria, D., Calabretta, M.M., Cevenini, L., Michelini, E., 2014a. Analyst 139, 6494–6501.
Roda, A., Michelini, E., Cevenini, L., Calabria, D., Calabretta, M.M., Simoni, P., 2014b. Anal. Chem. 86, 7299–7304.
Roda, A., Michelini, E., Zangheri, M., Di Fusco, M., Calabria, D., Simoni, P., 2016a. TrAC 79, 317–325.
Roda, A., Mirasoli, M., Michelini, E., Di Fusco, M., Zangheri, M., Cevenini, L., Roda, B., Simoni, P., 2016b. Biosens. Bioelectron. 76, 164–179.
Roggo, C., van der Meer, J.R., 2017. Curr. Opin. Biotechnol. 45, 24–33.
Sicard, C., Glen, C., Aubie, B., Wallace, D., Jahanshahi-Anbuhi, S., Pennings, K., Daigger, G.T., Pelton, R., Brennan, J.D., Filipe, C.D., 2015. Water Res. 70, 360–369.
Thouand, G., 2018. Anal. Bioanal. Chem. 410, 1189–1190.
Turner, A.P., 2013. Chem. Soc. Rev. 42, 3184–3196.
Wang, Q.X., Xue, S.F., Chen, Z.H., Ma, S.H., Zhang, S., Shi, G., Zhang, M., 2017. Biosens. Bioelectron. 15, 388–393.
WHO, 2003. Isoproturon in drinking-water. Background document for preparation of WHO Guidelines for drinking-water quality. Geneva, World Health Organization (WHO/SDE/WSH/03.04/37).
Wittig, R., Richter, V., Wittig-Blaich, S., Weber, P., Strauss, W.S., Bruns, T., Dick, T.P., Schneckenburger, H.J., 2013. Biomol. Screen. 18, 736–743.
Zhang, D., Liu, Q., 2016. Biosens. Bioelectron. 75, 273–284.